journal

J. Am. Ceram. Soc., 99 [10] 3343–3349 (2016)
DOI: 10.1111/jace.14356

Effect of Ordering on the Microwave Dielectric Properties of Spinel-Structured $(Zn_{1-x}(Li_{2/3}Ti_{1/3})_x)_2TiO_4$ Ceramics

Jian Zhang and Ruzhong Zuo†

Institute of Electro Ceramics and Devices, School of Materials Science and Engineering, Hefei University of Technology, Hefei 230009, China

Spinel-structured $(Zn_{1-x}(Li_{2/3}Ti_{1/3})_x)_2TiO_4$ (x = 0–1) microwave dielectric ceramics were manufactured via a conventional mixed-oxide method. The X-ray diffraction and Raman spectra revealed that a disordered face-centered cubic phase was found in the composition range of $x < 0.5$, and an ordered primitive cubic spinel solid solution was achieved as x was beyond 0.5. Such a disorder–order transition near $x = 0.5$ was accompanied by the variation of composition-induced cation occupancy. The $Q \times f$ value first kept increasing up to ~160 000 (GHz) in disordered ceramics, and then sharply decreased as an ordered structure appeared at $x \geq 0.5$. An obvious decrease in τ_f value was also accompanied by the appearance of an ordered structure. The minimum τ_f value (~ −20 ppm/°C) was obtained in the $x = 0.75$ sample with the highest structural order degree. These results demonstrated that microwave dielectric properties of current spinel ceramics could be successfully modified by adjusting their structural order degree, which could be appropriately adopted for the design of spinel-structured materials with favorable properties.

Keywords: *dielectric materials/properties; X-ray methods; Raman spectroscopy*

I. Introduction

The emerging progress and revolutionary changes in microwave telecommunication over the past decades have continuously stimulated the development of advanced integration, packaging, and interconnection technologies.[1,2] Particularly, significant progress in satellite communications and cell phone base stations speeds up the needs for new low-cost, moderate permittivity (ε_r) materials with a high quality factor ($Q \times f$) and a near-zero temperature coefficient of resonant frequency (τ_f).[1,3]

Li_2O–ZnO–TiO_2 ternary system has shown great potentials in lithium ion batteries,[4,5] solid electrolytes,[6] catalytic sorbents[7] and especially, as microwave dielectrics[2,8–10] for its advantages of low-cost raw materials, relatively low densification temperature, and low bulk density compared to other commercially available ceramics. Typically, a temperature-stable microwave dielectric $Li_2ZnTi_3O_8$ with an ordered spinel structure ($P4332$) and favorable properties of $\varepsilon_r = 25.6$, $Q \times f = 72{,}000$ GHz at 1075°C was proposed by George et al.[8] For medium permittivity microwave dielectrics, pure Zn_2TiO_4 (Fd-3m) with $\varepsilon_r = 21$ possessed good dielectric properties of $Q \times f = 50{,}000$ GHz and $\tau_f = -60$ ppm/°C at a relatively low sintering temperature of 1100°C.[9] Zhou et al. also introduced a new low-loss cubic spinel (Fd-3m) microwave dielectric ceramic $Li_2Zn_3Ti_4O_{12}$ with excellent microwave dielectric properties ($\varepsilon_r = 20.6$, $Q \times f = 106{,}700$ GHz, $\tau_f = -48$ ppm/°C at 1075°C).[10] The above-mentioned three typical compounds Zn_2TiO_4, $Li_2Zn_3Ti_4O_{12}$, and $Li_2ZnTi_3O_8$ correspond well with the compositions with x = 0, 0.5 and 0.75 of $Li_{1.33x}Zn_{2-2x}Ti_{1+0.67x}O_4$ (x = 0–1) in $ZnTi_2O_4$–$Li_4Ti_5O_{12}$ system, respectively. According to the relevant phase diagram,[11] there existed a phase transition from the primitive cubic (pc) to face-centered cubic (fcc), accompanied by the variation of structural order degree. It was thus anticipated that the order degree might be closely related to excellent microwave dielectric properties in lithium-based spinel.

In this study, a typical spinel-structured $[Zn_{1-x}(Li_{2/3}Ti_{1/3})_x]_2TiO_4$ (x = 0–1) system (abbreviated as ZLTT) was fabricated via a conventional solid-state route. The relationship between the variation of structural order degree and corresponding microwave dielectric properties was then discussed in detail by means of X-ray diffraction (XRD) and Raman spectroscopy.

II. Experimental Procedure

ZLTT (x = 0–1) ceramics were prepared via a conventional solid-state reaction method using high-purity (>99.9%) ZnO, TiO_2, and Li_2CO_3. It is worth noting that ZnO and TiO_2 tended to appear in stoichiometric Zn_2TiO_4 (x = 0) and $Li_4Ti_5O_{12}$ (x = 1) as a result of the difficult solid-state diffusion and lithium volatilization, respectively.[9,12–14] The existence of the secondary phase would interfere with the analysis on the structure and inherent microwave dielectric properties of ZLTT. By comparison, the effect from the non-stoichiometry might be neglected.[9,12,14] Thereby, an excess of 5 mol% TiO_2 was added for $x < 0.5$ samples[9] and 10 mol% TiO_2 was absent for the $x = 1$ sample.[14] The powder mixtures were weighed and then ball-milled with zirconia balls and polyethylene jars in alcohol for 4 h. The mixtures were dried, calcined at 850°C–950°C for 4 h in air, and then remilled for 6 h. The ground powders were granulated with 5 wt% of a poly (vinyl alcohol) solution as a binder, and then pressed into cylindrical pellets of ~10 mm in diameter with varying thicknesses (~1 mm for disks, ~5 mm for resonators). The pellets were first heated at 550°C in air for 4 h to burn out the organic binder, and then sintered over a temperature range of 1025°C–1150°C for 4 h, except that the $x = 1$ sample was sintered at 980°C for 4 h. The heating rate was 5°C/min, and the cooling rate was 10°C/min. To prevent the lithium evaporation, the compacts were muffled with powders of the same composition.

Room-temperature XRD was performed with Cu$K\alpha$ radiation at an acceleration condition of 40 kV and 30 mA (D/Max2500V; Rigaku, Tokyo, Japan). Before the examination, the sintered pellets were crushed into powders with a mortar. The diffraction patterns were obtained over a 2θ range of 10°–90° with a step of 0.02°. Structural characteristics of ZLTT compositions were studied with the help of Rietveld refinement using GSAS suite equipped with EXPGUI

A. Feteira—contributing editor

Manuscript No. 37991. Received December 31, 2015; approved May 15, 2016.
†Authors to whom correspondence should be addressed. e-mails: piezolab@hfut.edu.cn and rzzuo@hotmail.com

software.[15,16] The bulk densities of the sintered ceramics were measured using the Archimedes method. The microstructure of the sintered samples was observed by scanning electron microscopy (SEM; JSM-6490LV, JEOL, Tokyo, Japan) equipped with an energy-dispersive spectrometer (EDS). Before the SEM observation, the fractured surface was polished and thermally etched for 30 min. Raman spectra were measured for the sintered samples at room temperature using a Raman spectrometer (532 nm, Lab Ram, HR Evolution, HORIBA JOBIN YVON, Longjumeau Cedex, France). The full width at half maximum (FWHM) of Raman shifts was obtained by PEAKFIT using Gauss function. Microwave dielectric properties were measured by the Hakki-Coleman method and the TE_{018}-shield cavity method with a network analyzer (N5230C; Agilent, Palo Alto, CA). The τ_f values of the samples were measured in the temperature range from 20°C to 80°C. It can be calculated as follow:

$$\tau_f = \frac{f_2 - f_1}{f_1(T_2 - T_1)} \quad (1)$$

where f_1 and f_2 represent the resonant frequencies at T_1 and T_2, respectively.

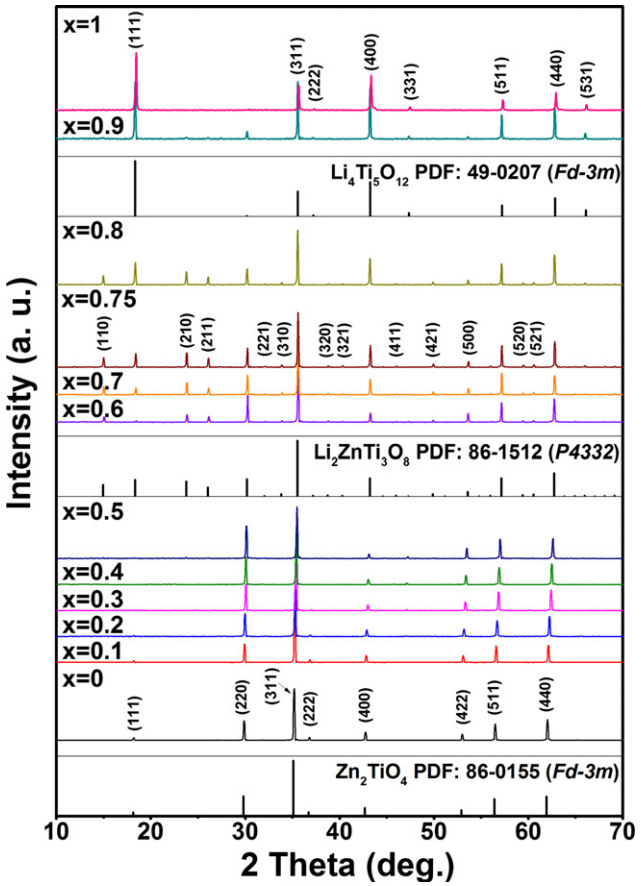

Fig. 1. XRD patterns of ZLTT ceramics sintered at optimal temperatures.

III. Results and Discussion

(1) Crystal Structure Characterization

The XRD patterns of ZLTT specimens sintered at their optimal temperatures are shown in Fig. 1. All the observed diffraction peaks for compositions with $0 \le x \le 0.5$ could be well indexed according to a disordered *fcc*-spinel Zn_2TiO_4 crystal (PDF# 86-0155), which belongs to *Fd*-3*m* space group. However, when $x > 0.5$, an additional set of diffraction peaks (110) (210) (221) (310) (421) (520) and (521) *etc.* appeared, which demonstrated the occurrence of *fcc–pc* phase transition, accompanied by a decreased structural symmetry.[11] These superlattice diffraction peaks also indicated the existence of an ordered *pc*-spinel $Li_2ZnTi_3O_8$ crystal (PDF# 86-1512) with a space group of *P*4332.[6] As is well-known, the structural order degree should increase with the increment of the intensity of superlattice diffraction peaks.[17] It could be seen that the intensity of typical peak (210) ($I_{(210)}$ for short) increased to the maximum at $x = 0.75$ with increasing x, suggesting this composition owns a structure with the highest order degree, which was also confirmed by the Raman analysis. In addition, it is worth noting that the main peak (311) moved toward higher angles with increasing x when $x < 0.9$, implying a decrement in unit cell volume, which was ascribed to the smaller ionic size of $(Li_{2/3}Ti_{1/3})^{2+}$ ($r_{AV} = 0.708$ Å) than that of Zn^{2+} ($r_{Zn2+} = 0.74$ Å).[18] Afterwards, when x reached 0.9, the main phase changed to another disordered *fcc*-spinel $Li_4Ti_5O_{12}$ crystal (PDF# 49-0207), which also belongs to *Fd*-3*m* space group. Some weak peaks belonging to the previous *pc*-spinel could also be observed until pure $Li_4Ti_5O_{12}$ was formed in the $x = 1$ sample.

(2) Rietveld Refinement

In order to analyze the structure transformation in more details, the schematic representation of spinel structure transition is illustrated in Fig. 2. The Rietveld refinement was carried out on XRD data of ZLTT compounds. Zn_2TiO_4 (ICSD# 80850, *Fd*-3*m* space group)[19] and $Li_2ZnTi_3O_8$ (ICSD# 82608, *P*4332 space group)[11] were chosen as the original models for $x = 0$–0.5 and $x = 0.6$–0.8 samples, respectively. The atomic occupancy of the initial models used for refinement was modified according to the Wyckoff site (marked in Fig. 2) and the composition. Detailed cation distribution in the structure of ZLTT is given in Table I. The ideal spinel structure should consist of a cubic close-packed

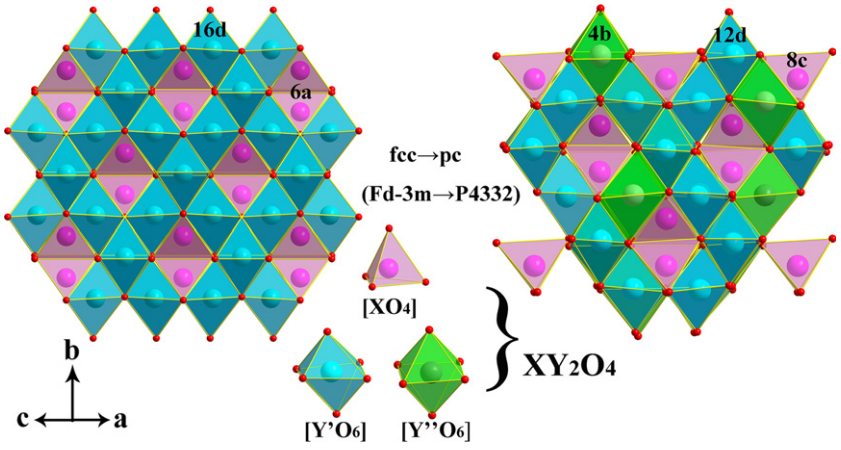

Fig. 2. Schematic representation of spinel structure transition from *fcc* to *pc* phase.

Table I. Occupancy of Cations at Tetrahedral and Octahedral Sites of ZLTT Ceramics

x	Space group	Tetrahedral site (X)		Octahedral site (Y2)				
	Fd-3*m*	8*a*			16*d*			
		Zn	Li			Zn	Ti	Li
0		1	0			0.5	0.5	0
0.1		1	0			0.4	0.53	0.07
0.2		1	0			0.3	0.57	0.13
0.3		1	0			0.2	0.6	0.2
0.4		1	0			0.1	0.63	0.27
0.5		1	0			0	0.667	0.333
1		0	1			0	0.833	0.167
	*P*4332	8*c*		4*b* (0.5)		12*d* (1.5)		
		Zn	Li	Li	Ti	Zn	Ti	Li
0.6		0.773	0.273	1	0	0.018	0.933	0.049
0.7		0.586	0.414	1	0	0.009	0.978	0.013
0.75		0.5	0.5	1	0	0	1	0
0.8		0.4	0.6	0.933	0.067	0	1	0

array of anions, with one-eighth of the tetrahedral and one-half of the octahedral interstices occupied by cations. It adopts a general formula $(X)_{Tet.}[Y_2]_{Oct.}O_4$ (X:Y = 1:2), where X and Y are tetrahedrally and octahedrally surrounded cations, respectively. Complex spinel phases allow either tetrahedral or octahedral site to be occupied by more than one kind of cations. As can be seen from Table I, in the compositions of $x \leq 0.5$ with *Fd*-3*m* space group, Wyckoff site 8*a* and 16*d* represent the positions of tetrahedral and octahedral center, respectively. It is believed that Zn^{2+} ions prefer to occupy 8*a* sites because of their near-zero octahedral site preference energy while other cations are randomly distributed in 16*d*, exhibiting a totally disordered state,[20] for instance, Zn_2TiO_4 could be written as $(Zn)_{Tet.}[ZnTi]_{Oct.}O_4$.[9] With x increasing, 16*d* site was firstly occupied by the substituted ions (Li, Ti) until completely filled at $x = 0.5$. The phase structure then transformed into *P*4332 space group when x was beyond 0.5. More specifically, the octahedral sites fell into 4*b* and 12*d* sites with a number ratio of 0.5:1.5, which were mainly occupied by Li^+ and Ti^{4+}. Meanwhile, these two sets of octahedral sites, Li_{4b} and Ti_{12d}, were spontaneously arranged into 1:3 cation ordering. Li^+ firstly filled the 4*b* site and then entered tetrahedral the 8*c* site, leading to the appearance of few Zn^{2+} in the 12*d* site. Also, of special note is that the $x = 0.75$ sample presented an ideal order. Nominally, $Li_2ZnTi_3O_8$ could be regarded as $(Li_{0.5}Zn_{0.5})_{Tet.}[Li_{0.5}Ti_{1.5}]_{Oct.}O_4$.[11] Afterwards, as x further increased, excess Ti^{4+} entered the 4*b* site, leading to the destruction of perfect octahedral order. As x continuously increased to one, Li^+ fully occupied tetrahedral sites while Ti^{4+} and residual Li^+ occupied octahedral sites, accompanying the formation of a completely disordered structure and the restoring of the space group to *Fd*-3*m*.

Bond valence is a weighted average according to the occupancy of each cation at its specific site. The Rietveld refinement plots and refined bond lengths for the $x = 0.4$ and 0.75 samples were chosen to illustrate the calculation of bond valence for each X and Y site by introducing the occupancy weight factor, as shown in Fig. 3 and Table II. The bond valence of the ions composing a unit cell was calculated by Eqs. (2–4):

$$v_{i-O} = \exp\left(\frac{R_{i-O} - d_{i-O}}{b}\right) \tag{2}$$

$$V_i = \sum v_{i-O} \tag{3}$$

$$V_Y = \sum V_i w_i \tag{4}$$

where $v_{i\text{-}O}$ is the bond valence between i cation and oxygen ion, $R_{i\text{-}O}$ is the bond valence parameter, $d_{i\text{-}O}$ is the bond length between atoms i and O, b is commonly taken to be a universal constant equal to 0.37 Å,[21] V_i is the sum of all the valences from a given cation i, V_Y is the sum of all the valences from the cations in Y site, and w_i is the occupying weight factor equal to the refined occupancy. In the $x = 0.4$ sample, there were three ions in the 16*d* site, so the bond valence of octahedral Y site could be calculated as follows:

$$V_Y = V_{Zn}w_{Zn} + V_{Ti}w_{Ti} + V_{Li}w_{Li} \tag{5}$$

Refined lattice parameters and bond valences of ZLTT are given in Table III. The refinement reliable factors of R_{wp},

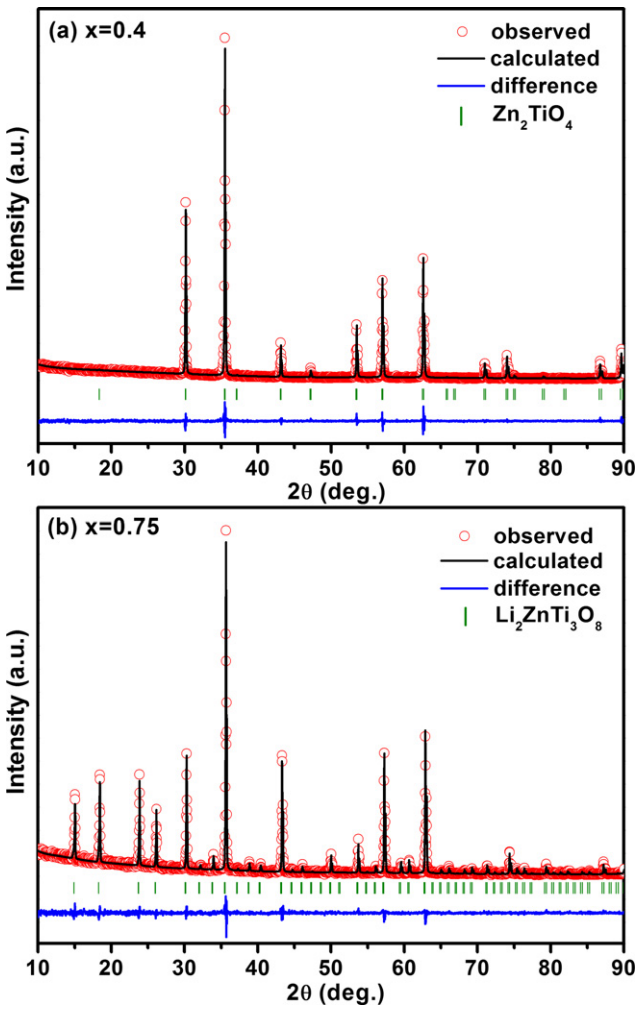

Fig. 3. Rietveld refinement plots of (a) $x = 0.4$ and (b) $x = 0.75$ ceramics.

R_p, and χ^2 were found to be in the range of 8%–13%, 6%–10%, and 1.4–2.1, respectively, indicating that the structural model was valid and the refinement result was reliable. As x increased, the unit cell volume and theoretical density decreased monotonously. It is noteworthy that the bond valence of X, Y, and O fluctuated in the disordered compositions within the range of $x \leq 0.5$, but afterwards, V_Y and V_O both increased to the maximum at $x = 0.75$ and then decreased with further increasing x, keeping consistent with the variation of the order degree. These results revealed the correspondence between V_Y and the ordered arrangement in octahedral sites. In addition, the decrement of V_X in the composition of $x > 0.5$ mainly resulted from the entrance of lower valence Li^+ than Zn^{2+} into the tetrahedral site. These parameters would be used to figure out the variation of microwave dielectric properties.

(3) Raman Spectrum Study

Raman spectroscopy is a powerful tool to probe the local crystal structure, short-range order, and more specific cation occupancy site. Moreover, it provides the information that correlates the vibrational characteristics to the microwave dielectric properties.[23] Therefore, Raman spectroscopy has been carefully performed on ZLTT ceramics and the results are shown in Fig. 4.

Only 7 and 12 modes could be observed in the typical disordered fcc phase and ordered *pc* phase for the samples with $x = 0$ and 0.75, respectively, which agreed well with the previous reports.[23,24] It is of importance in current work that the mode at ~718 cm^{-1} was due to symmetric breathing of $[TiO_6]$ and the mode observed at ~402 cm^{-1} could be assigned to $A_{1\ g}$ mode of $[ZnO_4]$ in $Li_2ZnTi_3O_8$.[23–27] With x increasing, the modes at 402 and 825 cm^{-1} appeared and increased in the disordered Zn_2TiO_4 spectrum, accompanying the decline of the modes of Zn_2TiO_4 at 304, 355, 480 cm^{-1} etc. This suggested the appearance and expansion of the short-range order, together with a growing number of lithium into octahedral sites. When $x > 0.5$, the structure changed to the long-range order, which could be clearly presented with the superlattice diffraction peaks in XRD.

Table II. Structure Refinement Parameters and Bond Valences of $x = 0.4$ Sample

Atom		Site	Occ.	Distance to O1/Å	Bond valence
X	Zn1	8*a*	1	1.95908(1) × 4	2.008
Y	Zn2	16*d*	0.1	2.02332(2) × 6	2.764
	Ti1	16*d*	0.63		
	Li1	16*d*	0.27		
O	O1	32*e*	1		1.884

Moreover, FWHM of A_{1g} $[ZnO_4]$ mode at 402 cm^{-1} presented the minimum value in the $x = 0.75$ sample with the highest order degree (discussed infra), probably because the intense and narrow Raman shifts are usually observed in well-ordered structure.[23] Furthermore, the appearance of the 825 cm^{-1} line might be explained by a severe distortion of $[TiO_6]$, since Coulomb repulsion in the presence of vast numbers of $[LiO_6]$ sharing edges with $[TiO_6]$ led to the shortening of some Ti–O bonds and hence to a higher vibration frequency.[6] This peak increased to the maximum at $x = 0.5$, then declined and even disappeared at $x = 0.75$ because its perfectly ordered structure owned the shortest bond and the highest bond strength, which was consistent with the variation of calculated V_Y in Table III. Additionally, with the increment of x, the A_{1g} mode of $[TiO_6]$ firstly shifted to the higher wave number side, then shifted to the lower side, and finally went back. The initial redshift could be attributed to the decrease of reduced mass (increased Li on octahedral sites) and vice versa,[23] which could be referred to the refined cation occupancy. Afterwards, as $x > 0.9$, 7 modes belonging to the disordered fcc phase $Li_4Ti_5O_{12}$ appeared, which are in good agreement with those reported by Julien et al.[28] Nevertheless, a little residual *fcc* phase could also be observed in Raman spectra of the $x = 0.9$ sample, such as 112, 402, and 520 cm^{-1} *etc.*, These further confirmed the above-mentioned phase evolution in XRD (Fig. 1).

(4) Microstructure Analysis

The microstructure of the ZLTT ceramics sintered at 1100°C (x = 0–0.6) and 1075°C (x = 0.75) for 4 h is

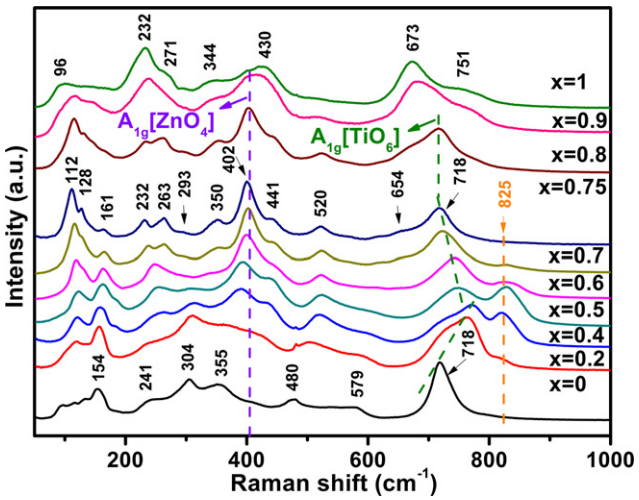

Fig. 4. Raman spectra of ZLTT ceramics sintered at optimal temperatures.

Table III. Rietveld Refinement Results and Bond Valence of ZLTT Ceramics

x	V_c (Å^3)	a (Å)	ρ(g/cm^3)	V_X	V_Y	V_O	R_{wp}(%), R_p(%), χ^2
0	606.28 (7)	8.4637 (3)	5.317	1.964	2.835	1.909	12.2, 9.03, 1.742
0.1	602.91 (6)	8.4479 (3)	5.143	1.880	2.889	1.915	10.7, 8.13, 2.077
0.2	600.17 (1)	8.43512 (8)	4.981	1.928	2.853	1.909	10.28, 7.9, 1.982
0.3	596.27 (1)	8.41689 (7)	4.807	1.820	2.933	1.922	9.89, 7.54, 1.785
0.4	593.37 (1)	8.40313 (8)	4.624	2.008	2.764	1.884	9.55, 7.29, 1.611
0.5	590.54 (1)	8.38976 (5)	4.451	1.992	2.769	1.882	8.92, 6.52, 1.418
0.6	588.86 (1)	8.38181 (9)	4.269	1.782	3.051	1.971	11.6, 8.79, 1.404
0.7	586.55 (2)	8.37083 (9)	4.076	1.416	3.364	2.036	13.06, 9.84, 1.62
0.75	586.71 (2)	8.36681 (9)	3.980	1.312	3.440	2.048	12.28, 9.12, 1.463
0.8	585.04 (2)	8.36364 (9)	3.883	1.144	3.399	1.985	12.8, 9.69, 1.565
1†	584.02 (1)	8.3588 (0)	3.311	0.948	3.395	1.935	—

ρ, theoretical density; R_{wp}, the reliability factor of weighted patterns; R_p, the reliability factor of patterns; χ^2, goodness-of-fit indicator = $(R_{wp}/R_{exp})^2$.
†Values from Ref. [22].

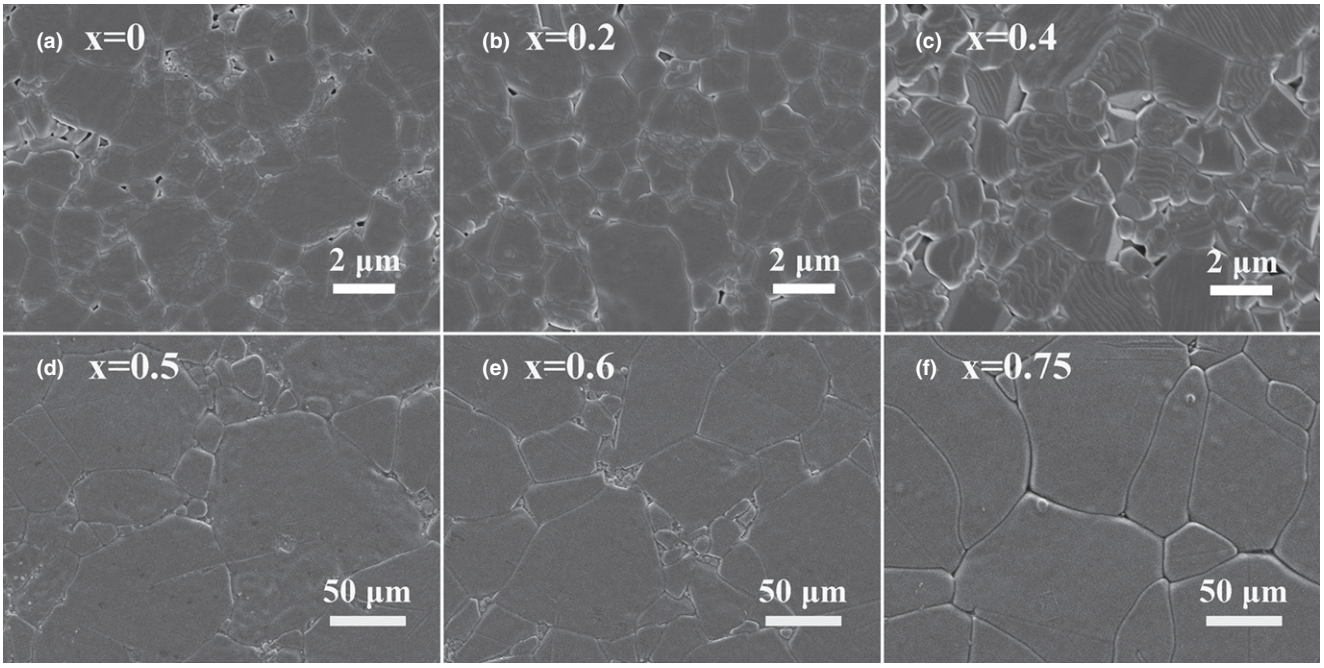

Fig. 5. SEM micrographs of polished and thermally etched ZLTT ceramics: (a) $x = 0$, (b) $x = 0.2$, (c) $x = 0.4$, (d) $x = 0.5$, (e) $x = 0.6$ sintered at 1100°C, and (f) $x = 0.75$ sintered at 1075°C.

illustrated in Fig. 5. It could be observed that the fine grains (2–4 μm) were closely packed with a small amount of pores for the samples with $x = 0$–0.4, and while for $x \geq 0.5$, the average grain size dramatically increased up to ~150 μm, accompanying the disappearance of pores. Moreover, some small grains could also be seen at the boundary of these large grains. The EDS results showed that the small and large grains had an identical composition (not listed here). Micrographs of the compounds with $x = 0$, 0.5, and 0.75 were exactly consistent with those reported by Refs. [8–10]. An obvious variation in grain size between $x = 0.4$ and 0.5 might be related to the disorder to order phase structure transition.

(5) Structure and Property Analysis

Figure 6 shows the variation of relative density, ε_r and ionic polarizability (α_D) of ZLTT ceramics sintered at different temperatures. As can be seen from Fig. 6(a), all the specimens were well sintered with high-density values (beyond 94%) at their optimal temperatures of 1125°C ($x = 0$–0.1), 1100°C ($x = 0.2$–0.3), 1075°C ($x = 0.4$), 1050°C ($x = 0.5$–0.9), and 980°C ($x = 1$), indicating that the substitution of $(Li_{2/3}Ti_{1/3})^{2+}$ for Zn^{2+} effectively reduced the sintering temperature of Zn_2TiO_4 matrix. In addition, the variation of ε_r as a function of sintering temperature was consistent with that of density as shown in Fig. 6(b). On the other hand, along with the increase of x, ε_r value of ZLTT decreased slightly when $x \leq 0.5$ and increased afterwards, corresponding to the *fcc* and *pc* region, respectively. Generally, ε_r mainly depends on the density, ionic polarizability, microstructure, porosity, and secondary phase.[29] The ionic polarizability could be calculated with the Clausius–Mossotti equation:

$$\alpha_D = \frac{3V_m(\varepsilon_r - 1)}{4\pi(\varepsilon_r + 2)} \quad (6)$$

where V_m is molar volume, which is determined from the unit cell volume (V_c) and formula number Z ($Z = 8$).[30] As expected, the composition dependence of α_D was consistent with that of ε_r, as seen in the inset of Fig. 6(b). Therefore, density and ionic polarizability might be responsible for the changes of ε_r in current system.

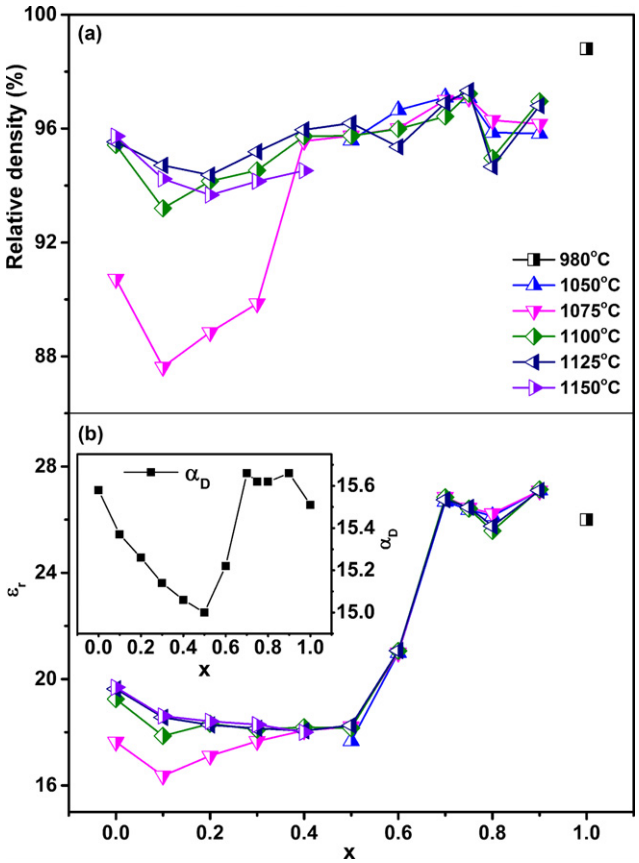

Fig. 6. Variation of relative density, ε_r and α_D of ZLTT ceramics at different temperatures.

The variation in $Q \times f$ value and packing fraction of the ZLTT solid solution is demonstrated in Fig. 7. As is well-known, the $Q \times f$ value depends on the intrinsic and extrinsic factors. The former is associated with lattice anharmonicity, which is mainly affected by a particular composition and crystal structure of the materials. The latter is related with density, impurity, secondary phase, grain size,

etc. According to Kim et al.,[31] the $Q \times f$ value is also largely dependent on the packing fraction (PF) defined by summing the volume of packed ions (V_{PI}) over the volume of a primitive unit cell as follows:

$$PF(\%) = \frac{V_{PI}}{V_c} \times Z \quad (7)$$

where V_{PI} is dependent on the occupation of refinement in Table I. As the packing fraction increased, the intrinsic loss decreased with the weakened lattice vibrations, leading to the improved $Q \times f$ value.[31] Hence, the enhancement of $Q \times f$ values for the samples in the composition range of $x = 0$–0.5 was primarily assigned to the packing fraction. However, when $x > 0.5$, the $Q \times f$ value abruptly decreased in spite of the continuously increasing packing fraction. The reason might be that spinel structure transformed from disordered *fcc* to ordered *pc* phase beyond $x = 0.5$. As a result, the special ordered structure would frame lithium ion transport channel to increase the conductivity and conduction loss,[6] leading to the decrease of $Q \times f$ value. For example, lithium could move from the tetrahedral site 8*c* to the vacant octahedral site in $Li_2ZnTi_3O_8$ ($P4332$).[6]

The τ_f value is also a key parameter for dielectric resonator materials, which predominantly depends on phase composition and structure characteristics such as octahedral distortion, structure ordering, and bond valence of oxygen/cations.[32,33] In current work, the τ_f value changed a little in *fcc* phase, but increased from −55 to −42 ppm/°C as $x > 0.5$, accompanying the phase transition to *pc*-spinel. It was supposed that τ_f in *pc*-spinel might have some relevance to the order degree and structure characteristics. Figure 8 describes the variation of τ_f and V_Y for ZLTT ($x = 0.5$–1) solid solutions. The inset shows the variation of above-mentioned $I_{(210)}$ and FWHM in *pc* phase region. Both the largest $I_{(210)}$ and smallest FWHM disclosed the highest order degree at $x = 0.75$. Meanwhile, this sample also exhibited the largest V_Y. It is speculated that the larger V_Y was probably related to the increased order degree. In addition, a similar variation trend with x was found for τ_f and V_Y. A larger V_Y usually means a higher bond energy, which would lead to a more stable system and a bigger force to recover the tilting of [YO_6] octahedron.[33] As a result, the absolute value of τ_f decreased. Similar results have also been demonstrated by Reaney et al. and Zhang et al.[34–36] In brief, the variation of τ_f value is closely related to the degree of structural order, as manifested by the bond valence or bond energy of the octahedron in a spinel structure.

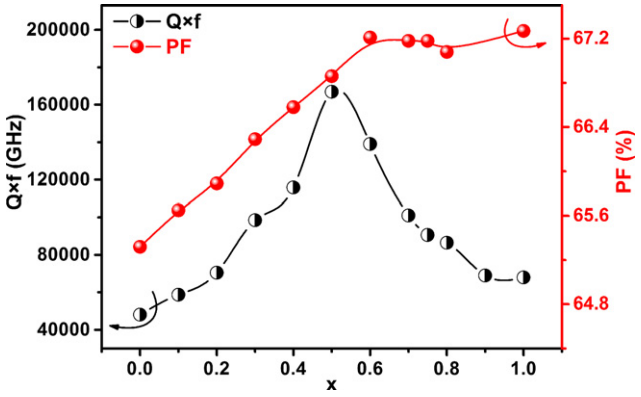

Fig. 7. Variation of $Q \times f$ and packing fraction of ZLTT ceramics at optimal temperatures.

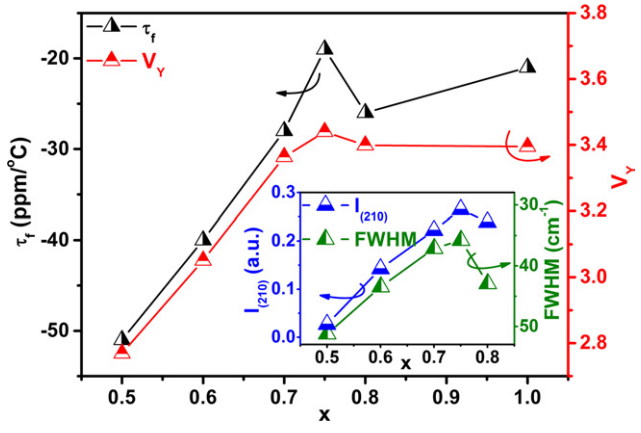

Fig. 8. Correlation among τ_f, V_Y, $I_{(210)}$, and FWHM of ZLTT ($x = 0.5$–1) ceramics.

IV. Conclusions

Spinel-structured ZLTT ($x = 0$–1) solid solutions were successfully prepared via a conventional ceramic route and their dielectric properties were investigated within the microwave frequency region. A disordered *fcc* phase was found in the composition range of $x < 0.5$ and an ordered *pc*-spinel solid solutions were achieved as $0.5 < x < 0.9$. Such a disorder–order transition near $x = 0.5$ was accompanied by the variation of composition-induced cation occupancy. The highest order degree appeared in the $x = 0.75$ sample. The increment of structural order was considered to bring more lithium ion transport channels and a more stable system, leading to a sharply decayed $Q \times f$ value and simultaneously a decreased τ_f value, respectively. These results demonstrated that microwave dielectric properties of current spinel ceramics were largely affected by adjusting their structural order degrees.

Acknowledgments

This work was financially supported by the National Natural Science Foundation of China (grant no. 51272060) and the Natural Science Foundation of Anhui Province (grant no. 1508085JGD04).

References

[1]M. T. Sebastian, *Dielectric Materials for Wireless Communications*. Elsevier Publishers, Oxford, 2008.
[2]S. George and M. T. Sebastian, "Low-Temperature Sintering and Microwave Dielectric Properties of $Li_2ATi_3O_8$ (A=Mg, Zn) Ceramics," *Int. J. Appl. Ceram. Technol.*, **8** [6] 1400–7 (2011).
[3]J. Zhang, Z. X. Yue, Y. Y. Zhou, X. H. Zhang, and L. T. Li, "Microwave Dielectric Properties and Thermally Stimulated Depolarization Currents of $(1-X)MgTiO_3$–$XCa_{0.8}Sr_{0.2}TiO_3$ Ceramics," *J. Am. Ceram. Soc.*, **98** [5] 1548–54 (2015).
[4]K. Mukai, Y. Kato, and H. Nakano, "Understanding the Zero-Strain Lithium Insertion Scheme of $Li[Li_{1/3}Ti_{5/3}]O_4$: Structural Changes at Atomic Scale Clarified by Raman Spectroscopy," *J. Phys. Chem. C*, **118** [6] 2992–9 (2014).
[5]F. C. Qie and Z. Y. Tang, "Cu-Doped $Li_2ZnTi_3O_8$ Anode Material with Improved Electrochemical Performance for Lithium-Ion Batteries," *Mater. Express*, **4** [3] 221–7 (2014).
[6]I. A. Leonidov, O. N. Leonidova, R. F. Samigullina, and M. V. Patrakeev, "Structural Aspects of Lithium Transfer in Solid Electrolytes $Li_{2x}Zn_{2-3x}Ti_{1+x}O_4$ ($0.33 \le x \le 0.67$)," *J. Struct. Chem.*, **45** [2] 262–8 (2004).
[7]U. Steinike and B. Wallis, "Formation and Structure of Ti-Zn-Oxides," *Cryst. Res. Technol.*, **32** [1] 187–93 (1997).
[8]S. George and M. T. Sebastian, "Synthesis and Microwave Dielectric Properties of Novel Temperature Stable High Q, $Li_2ATi_3O_8$ (A=Mg, Zn) Ceramics," *J. Am. Ceram. Soc.*, **93** [8] 2164–6 (2010).
[9]H. T. Kim, Y. Kim, M. Valant, and D. Suvorov, "Titanium Incorporation in Zn_2TiO_4 Spinel Ceramics," *J. Am. Ceram. Soc.*, **84** [5] 1081–6 (2001).
[10]H. F. Zhou, X. B. Liu, X. L. Chen, L. Fang, and Y. L. Wang, "$ZnLi_{2/3}Ti_{4/3}O_4$: A New Low Loss Spinel Microwave Dielectric Ceramic," *J. Eur. Ceram. Soc.*, **32** [2] 261–5 (2012).
[11]V. S. Hernandez, L. M. T. Martinez, G. C. Mather, and A. R. West, "Stoichiometry, Structures and Polymorphism of Spinel-Like Phases, $Li_{1.33x}Zn_{2-2x}Ti_{1+0.67x}O_4$," *J. Mater. Chem.*, **6** [9] 1533–6 (1996).
[12]H. T. Kim, J. D. Byun, and Y. Kim, "Microstructure and Microwave Dielectric Properties of Modified Zinc Titanates (II)," *Mater. Res. Bull.*, **33** [6] 975–86 (1998).
[13]S. S. Cole and W. K. Nelson, "The System Zinc Oxide-Titanium Dioxide. Zinc Orthotitanate and Solid Solutions with Titanium Dioxide," *J. Phys. Chem.*, **42** [2] 245–51 (1938).
[14]J. Zhang, R. Z. Zuo, Y. Wang, and S. S. Qi, "Phase Evolution and Microwave Dielectric Properties of $Li_4Ti_{5(1+x)}O_{12}$ Ceramics," *Mater. Lett.*, **164**, 353–5 (2016).

[15]A. C. Larson and R. B. Von Dreele, General Structural Analysis System (GSAS), Report LAUR 86-748, Los Alamos National Laboratory, Los Alamos, New Mexico, 2000.
[16]B. H. Toby, "EXPGUI, a Graphical User Interface for GSAS," *J. Appl. Crystallogr.*, **34** [2] 210–3 (2001).
[17]J. J. Bian and Y. F. Dong, "New High Q Microwave Dielectric Ceramics with Rock Salt Structures: $(1-x)Li_2TiO_3+XMgO$ System ($0 \le x \le 0.5$)," *J. Eur. Ceram. Soc.*, **30** [2] 325–30 (2010).
[18]R. D. Shannon, "Revised Effective Ionic Radii and Systematic Studies of Interatomic Distances in Halides and Chalcogenides," *Acta Cryst. A*, **32** [5] 751–67 (1976).
[19]R. L. Millard, R. C. Peterson, and B. K. Hunter, "Study of the Cubic to Tetragonal Transition in Mg_2TiO_4 and Zn_2TiO_4 Spinels by 17O MAS NMR and Rietveld Refinement of X-ray Diffraction Data," *Am. Miner.*, **80** [9–10] 885–96 (1995).
[20]H. Kawai, M. Tabuchi, M. Nagata, H. Tukamoto, and A. R. West, "Crystal Chemistry and Physical Properties of Complex Lithium Spinels $Li_2MM'_3O_8$ (M=Mg, Co, Ni, Zn; M′=Ti, Ge)," *J. Mater. Chem.*, **8** [5] 1273–80 (1998).
[21]N. E. Brese and M. O'keeffe, "Bond-Valence Parameters for Solids," *Acta Cryst. B*, **47** [2] 192–7 (1991).
[22]M. Nakayama, Y. Ishida, H. Ikuta, and M. Wakihara, "Mixed Conduction for the Spinel Type $(1-x)Li_{4/3}Ti_{5/3}O_4$-$XLiCrTiO_4$ System," *Solid State Ionics*, **117** [3–4] 265–71 (1999).
[23]S. K. Singh, S. R. Kiran, and V. R. K. Murthy, "Structural, Raman Spectroscopic and Microwave Dielectric Studies on Spinel $Li_2Zn_{(1-x)}Ni_xTi_3O_8$ Compounds," *Mater. Chem. Phys.*, **141** [2–3] 822–7 (2013).
[24]D. Wongratanaphisan, T. Santhaveesuk, and S. Choopun, "Raman Scattering of Internal Dynamics in Spinel Zn_2TiO_4 Nanostructures," *Integr. Ferroelectr.*, **142** [1] 37–43 (2013).
[25]Z. Wang, S. K. Saxena, and C. S. Zha, "In Situ X-ray Diffraction and Raman Spectroscopy of Pressure-Induced Phase Transformation in Spinel Zn_2TiO_4," *Phys. Rev. B*, **66** [2] 024103, 5pp (2002).
[26]K. R. Zhu, M. S. Zhang, Q. Chen, and Z. Yin, "Size and Phonon-Confinement Effects on Low-Frequency Raman Mode of Anatase TiO_2 Nanocrystal," *Phys. Lett. A*, **340** [1–4] 220–7 (2005).
[27]R. Yang, H. Liu, Y. Wang, W. Jiang, X. Hao, et al., "Structure and Properties of ZnO-Containing Lithium–Iron–Phosphate Glasses," *J. Alloys Compd*, **513**, 97–100 (2012).
[28]C. M. Julien, M. Massot, and K. Zaghib, "Structural Studies of $Li_{4/3}Me_{5/3}O_4$ (Me=Ti, Mn) Electrode Materials: Local Structure and Electrochemical Aspects," *J. Power Sources*, **136** [1] 72–9 (2004).
[29]Q. W. Liao, L. X. Li, X. Ren, and X. Ding, "New Low-Loss Microwave Dielectric Material $ZnTiNbTaO_8$," *J. Am. Ceram. Soc.*, **94** [10] 3237–40 (2011).
[30]R. D. Shannon, "Dielectric Polarizabilities of Ions in Oxides and Fluorides," *J. Appl. Phys.*, **73** [1] 348–66 (1993).
[31]E. S. Kim, B. S. Chun, R. Freer, and R. J. Cernik, "Effects of Packing Fraction and Bond Valence on Microwave Dielectric Properties of $A^{2+}B^{6+}O_4$ (A^{2+}: Ca, Pb, Ba; B^{6+}: Mo, W) Ceramics," *J. Eur. Ceram. Soc.*, **30** [7] 1731–6 (2010).
[32]A. J. Bosman and E. E. Havinga, "Temperature Dependence of Dielectric Constants of Cubic Ionic Compounds," *Phys. Rev.*, **129** [4] 1593–600 (1963).
[33]H. J. Lee, K. S. Hong, S. J. Kim, and I. T. Kim, "Dielectric Properties of MNb_2O_6 Compounds (Where M = Ca, Mn, Co, Ni, or Zn)," *Mater. Res. Bull.*, **32** [7] 847–55 (1997).
[34]I. M. Reaney, E. L. Colla, and N. Setter, "Dielectric and Structural Characteristics of Ba- and Sr-Based Complex Perovskites as a Function of Tolerance Factor," *Jpn. J. Appl. Phys.*, **33** [7A] 3984–90 (1994).
[35]P. Zhang and Y. G. Zhao, "Effects of Structural Characteristics on Microwave Dielectric Properties of $Li_2Mg(Ti_{1-x}Mn_x)_3O_8$ Ceramics," *J. Alloys Compd*, **647**, 386–91 (2015).
[36]P. Zhang, Y. G. Zhao, and X. Y. Wang, "The Correlations Between Electronic Polarizability, Packing Fraction, Bond Energy and Microwave Dielectric Properties of $Nd(Nb_{1-x}Sb_x)O_4$ Ceramics," *J. Alloys Compd*, **644**, 621–5 (2015). □